



## NRC Publications Archive Archives des publications du CNRC

### **Self-assembly and visualization of poly(3-hexyl-thiophene) chain alignment along boron nitride nanotubes**

Martinez-Rubi, Yadienka; Jakubek, Zygmunt J.; Jakubinek, Michael B.; Kim, Keun Su; Cheng, Fuyong; Couillard, Martin; Kingston, Christopher; Simard, Benoit

This publication could be one of several versions: author's original, accepted manuscript or the publisher's version. / La version de cette publication peut être l'une des suivantes : la version prépublication de l'auteur, la version acceptée du manuscrit ou la version de l'éditeur.

For the publisher's version, please access the DOI link below. / Pour consulter la version de l'éditeur, utilisez le lien DOI ci-dessous.

#### **Publisher's version / Version de l'éditeur:**

<https://doi.org/10.1021/acs.jpcc.5b09049>

*The Journal of Physical Chemistry C*, 119, 47, pp. 26605-26610, 2015-11-06

#### **NRC Publications Record / Notice d'Archives des publications de CNRC:**

<https://nrc-publications.canada.ca/eng/view/object/?id=8cd2d56e-f828-4c35-add0-dae9126d1079>

<https://publications-cnrc.canada.ca/fra/voir/objet/?id=8cd2d56e-f828-4c35-add0-dae9126d1079>

Access and use of this website and the material on it are subject to the Terms and Conditions set forth at

<https://nrc-publications.canada.ca/eng/copyright>

READ THESE TERMS AND CONDITIONS CAREFULLY BEFORE USING THIS WEBSITE.

L'accès à ce site Web et l'utilisation de son contenu sont assujettis aux conditions présentées dans le site

<https://publications-cnrc.canada.ca/fra/droits>

LISEZ CES CONDITIONS ATTENTIVEMENT AVANT D'UTILISER CE SITE WEB.

**Questions?** Contact the NRC Publications Archive team at

PublicationsArchive-ArchivesPublications@nrc-cnrc.gc.ca. If you wish to email the authors directly, please see the first page of the publication for their contact information.

**Vous avez des questions?** Nous pouvons vous aider. Pour communiquer directement avec un auteur, consultez la première page de la revue dans laquelle son article a été publié afin de trouver ses coordonnées. Si vous n'arrivez pas à les repérer, communiquez avec nous à PublicationsArchive-ArchivesPublications@nrc-cnrc.gc.ca.



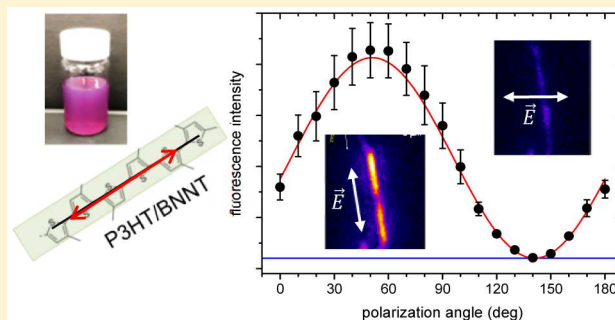
# Self-Assembly and Visualization of Poly(3-hexyl-thiophene) Chain Alignment along Boron Nitride Nanotubes

Yadienka Martinez-Rubi,<sup>†</sup> Zygmunt J. Jakubek,<sup>‡</sup> Michael B. Jakubinek,<sup>†</sup> Keun Su Kim,<sup>†</sup> Fuyong Cheng,<sup>†</sup> Martin Couillard,<sup>#</sup> Christopher Kingston,<sup>†</sup> and Benoit Simard<sup>\*,†</sup>

<sup>†</sup>Security and Disruptive Technologies, <sup>‡</sup>Measurement Science and Standards, and <sup>#</sup>Energy, Mining and Environment, National Research Council Canada, Ottawa, Ontario K1A 0R6, Canada

## Supporting Information

**ABSTRACT:** Boron nitride nanotubes (BNNTs) were non-covalently functionalized with poly(3-hexyl-thiophene) (P3HT) to produce stable suspensions. The conjugated polymer and BNNTs interact via  $\pi$ - $\pi$  stacking, and the resulting self-assembly of regiorandom P3HT on the BNNT surface is immediately evident through a color change and the appearance of a partially resolved absorption band. By employing polarized excitation fluorescence microscopy, we directly visualized the polymer-functionalized BNNTs and determined the conformation of the polymer on BNNT surfaces. Variation of fluorescence intensity with linear polarization direction showed conclusively that the P3HT chains were always aligned parallel to the BNNT long axis.



## INTRODUCTION

Boron nitride nanotubes (BNNTs) are structurally analogous to carbon nanotubes (CNTs) but offer a different set of properties such as higher thermal stability, high polarizability, wide band gap, and high neutron absorption cross section. These features make BNNTs attractive fillers for multifunctional polymer nanocomposites and offer advantages over CNTs in some cases. Such applications often require a stable and uniform dispersion, which can be achieved by modification of the BNNT surface. Noncovalent functionalization of BNNTs has been described using alkylamines, alkylphosphines,<sup>1</sup> aromatic containing molecules,<sup>2</sup> and polymers.<sup>3</sup> The interactions in these cases are mediated by electron-rich nitrogen or phosphorus species interacting with electron-deficient boron and by  $\pi$ - $\pi$  interactions. For example, conjugated poly[*m*-phenylenevinylene-*co*-(2,5-dioctoxy-*p*-phenylenevinylene)] noncovalently wraps BNNTs.<sup>3</sup> More recently, noncovalent functionalization of BNNTs using two conjugated poly(*p*-phenylene ethynylene)s (PPE) and a polythiophene (PT) derivative was reported, and the absorption/emission of the PPE derivatives attaching on BNNTs showed red shifts in comparison with free PPEs due to the enhanced planarization, while the PT derivative showed blue shifts suggesting a disruption of its  $\pi$ -conjugation.<sup>4</sup> While several conjugated polymers have been shown to functionalize BNNTs and improve solubility, the details of the interactions have not been fully studied.

PT derivatives have been more widely investigated for modification of CNTs.<sup>5-12</sup> Poly(3-hexyl-thiophene) (P3HT) was shown to wrap around single-walled CNTs in a number of

conformations such as helices, bundles, and more elongated conformations that maximize planar  $\pi$ - $\pi$  stacking.<sup>8</sup> Microscopic evidence of the P3HT coil wrapping around multiwalled CNTs (MWCNTs) also has been reported.<sup>9</sup> In contrast, several studies have shown that CNTs can serve as orientation templates and heterogeneous nucleation agents for formation of crystalline P3HT nanofibrils perpendicular to the CNT axis.<sup>10-12</sup> It has been shown that the thiophene rings provide a zigzag backbone that allows a thermodynamically more stable coaxial attachment on CNTs, providing an ordered growth front, while reports of wrapping are attributed to kinetic effects.<sup>12</sup> Disagreement between observations has been attributed to both complicated interactions and a lack of effective methods to assess the polymer conformation.<sup>12</sup> In this work, we employ P3HT to noncovalently functionalize BNNTs and demonstrate that polarized excitation fluorescence microscopy is a powerful method to assess the conformation of conjugated polymers on nanotube surfaces. Using this technique, we show conclusively that the P3HT chains were always aligned along the BNNT axis.

## EXPERIMENTAL SECTION

BNNTs were synthesized by a thermal plasma process.<sup>13</sup> High-quality, small-diameter ( $\sim 5$  nm) BNNTs were produced in high yield directly from hexagonal boron nitride (h-BN) powder (99.5%, avg. 70 nm, MK-hBN-N70, M K Impex Corp.)

Received: September 16, 2015

Revised: November 3, 2015

Published: November 6, 2015

and postpurified through thermal and solvent treatments. Regiorandom-P3HT (rra-P3HT;  $M_w = 60\text{--}90$  kDa) was obtained from Rieke Metals, Inc.

**P3HT/BNNT Suspensions.** The P3HT-functionalized BNNTs were prepared by suspending 3 mg of BNNTs in 15 mL of  $\text{CHCl}_3$  with the aid of bath sonication (15 min) and adding, dropwise, a solution of P3HT in  $\text{CHCl}_3$  (0.5 mg/mL). The mixture was bath-sonicated for 15 min.

**Absorption Spectroscopy.** Polymer, neat BNNT, and polymer-functionalized BNNT solutions and/or suspensions were characterized at various stages of the experiment by ultraviolet–visible (UV–vis) absorption spectroscopy. Spectra were recorded with a Cary 5000 spectrophotometer (Agilent) with solutions in 10 mm path length quartz cuvettes.

**Polarized Excitation Fluorescence Microscopy.** To elucidate the conformation of the rra-P3HT polymer on BNNT, we conducted a polarized excitation fluorescence microscopy investigation of the rra-P3HT/BNNT hybrids. A drop of a highly dilute rra-P3HT/BNNT suspension was spread on a piranha-cleaned no. 1.5 coverslip, excess suspension was removed with lens cleaning paper, and the sample was air-dried. The dilution was optimized to minimize aggregation of rra-P3HT/BNNT hybrids on the coverslip and ensure the distance between fluorescing features to be on the order of 3–5  $\mu\text{m}$  or approximately 10–20 times the diffraction limit. The sample was imaged by polarized excitation fluorescence microscopy using a fluorescence microscope based on the IX-81 Olympus platform. The sample was illuminated with a 543 nm He–Ne laser beam selected to maximize excitation of the rra-P3HT/BNNT hybrids and minimize excitation of free rra-P3HT. The beam was focused on the back focal plane of a 150 $\times$  oil immersion TIRF objective (UApo 150 $\times$ /1.45 oil TIRFM, Olympus) in order to obtain a well-collimated beam in the sample plane. The laser beam was linearly polarized with a variable direction of polarization in the sample plane controlled by a half wave plate (WPH05M-546, Thorlabs) installed in an optics slot directly beneath the objective. Fluorescence was collected by the objective and passed through a Semrock FF01-593/40-25 fluorescence filter, resulting in selective detection of the fluorescence in the 570–615 nm range. An optional 1.6 $\times$  lens was inserted in the detection path for a 240 $\times$  total magnification of the sample image. The fluorescence images were recorded using a Photometrics Evolve 512 Delta EMCCD camera with the excitation beam polarization rotated in either 10 or 20 $^\circ$  steps in the 0–180 $^\circ$  range with respect to the X axis (left-to-right direction as observed by the experimenter in front of the microscope).

## RESULTS AND DISCUSSION

As shown in Figure 1a, BNNTs were dispersed in chloroform after addition of rra-P3HT, and the orange color observed for the rra-P3HT solution changed instantaneously to purple. The color change indicates a significant change in the conformation of the polymer chains.<sup>14</sup> rra-P3HT/BNNT suspensions (0.2 mg/mL) are stable for weeks with only trace sedimentation. Absorption spectra are presented in Figure 1b. The supernatant of pristine BNNTs shows only weak scattering in the 300–700 nm region and no absorption because the BNNT band gap is in the UV ( $\sim 5.9$  eV). Absorbance of rra-P3HT/BNNT was significantly higher as compared with pristine BNNTs and had a much stronger scattering component, indicating that the  $\pi$ – $\pi$  interaction with rra-P3HT can effectively debundle BNNT aggregates and improve solubility. The spectrum of the orange

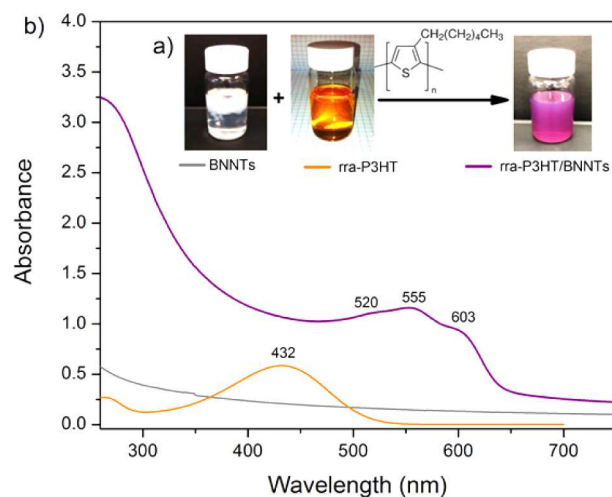


**Figure 1.** (a) Photos and (b) absorption spectra of BNNT (0.2 mg/mL), rra-P3HT solution, and rra-P3HT/BNNT suspensions in  $\text{CHCl}_3$  (rra-P3HT to BNNT weight ratio = 0.08).

rra-P3HT solution in  $\text{CHCl}_3$  (Figure 1b) contains one unstructured band (maximum at 432 nm) associated with the intrachain  $\pi$ – $\pi^*$  transition of well-dissolved rra-P3HT in a coil-like conformation.<sup>15</sup> By contrast, rra-P3HT/BNNTs display a significantly red-shifted band having a partially resolved structure with absorption peaks near 520, 555, and 603 nm. These changes suggest that chain twisting is strongly inhibited as a result of  $\pi$ – $\pi$  interactions leading to planar molecules with extended conjugation at the BNNT surface. Similar behavior is observed for regioregular-P3HT/BNNT (Figure S1), where corresponding bands are observed at slightly higher wavelengths (562 and 605 nm) due to a longer conjugation length.

The color and solubility changes of the BNNT suspension were examined as a function of the rra-P3HT to BNNT weight ratio (Figure 2). Immediately after adding orange-colored rra-P3HT solution (rra-P3HT to BNNT weight ratio = 0.008), the color changed to purple (Figure 2a), providing visual indication of planarization of the polymer chains at the BNNT interface. With an increasing amount of rra-P3HT added, BNNTs gradually dispersed (Figure 2a), and the UV–vis spectra (Figure 2b) showed only the longer-wavelength, structured band until the maximum BNNT concentration was achieved ( $\sim 0.08$ –0.1 rra-P3HT to BNNT weight ratio). At higher ratios, an additional band at 432 nm corresponding to free polymer appeared and increased with rra-P3HT content.

Figure 2c shows the evolution of absorption at 555 and 300 nm, which are measures of the concentration of rra-P3HT/BNNT hybrids and the degree of BNNT debundling, respectively, as functions of the weight ratio of rra-P3HT to BNNT. For weight ratios of rra-P3HT to BNNT of approximately 0.08–0.1 and greater, the absorption at 432 nm measures the concentration of rra-P3HT in solution not attached to the BNNTs. The evolution of this band intensity is also shown in Figure 2c. The relative intensity of the 603 nm band has been used to evaluate the degree of crystallinity of rra-P3HT/MWCNT composites<sup>8</sup> and P3HT nanowhiskers.<sup>16</sup> The intensity ratio for rra-P3HT/BNNT as a function of increasing P3HT to BNNT weight ratio is included in Figure 2c. The  $I_{603}/I_{555}$  ratio is approximately constant, indicating the formation of similar morphologies at the BNNT surface until all of the available BNNT surface is covered by the polymer ( $\sim 0.08$ –0.1 rra-P3HT to BNNT weight ratio), after which further addition

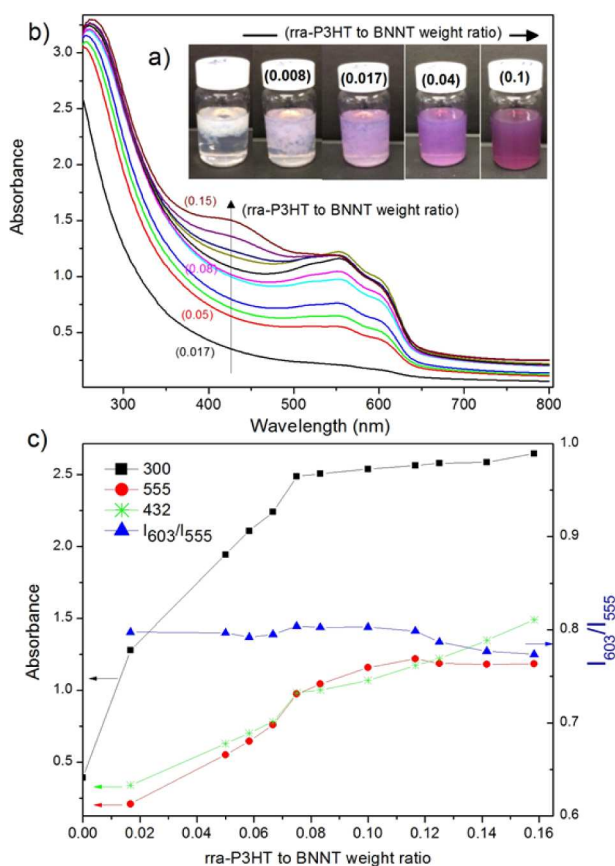


**Figure 2.** (a) Photos and (b) absorption spectra of rra-P3HT/BNNTs in  $\text{CHCl}_3$  at increasing rra-P3HT to BNNT weight ratio (indicated by the numbers in parentheses). (c) Evolution of the absorbance as a function of the rra-P3HT to BNNT ratio. Lines are added to guide the reader's eye.

only leaves rra-P3HT in solution in a coil-like conformation, as indicated by further increasing absorption at 432 nm and unchanged absorption at 555 nm. Estimates of the BNNT surface coverage by a single layer of polymer indicate ~20–50% coverage of the BNNT surface area at the 0.08 rra-P3HT to BNNT weight ratio (see the [Supporting Information](#)).

Molecular dynamics simulation has been used to investigate interfacial binding of BNNTs and CNTs with PT, revealing the PT/BNNT interactions to be much stronger.<sup>17</sup> Our experiments with MWCNTs show that rra-P3HT also debundles MWCNTs, and a weak broad band is observed (530–680 nm), indicating planarization and adsorption of rra-P3HT on the MWCNTs (Figure S2). However, the absorption band has a more diffuse structure than that for BNNTs under similar conditions. This could be due to a less uniform and broader conformation distribution on the CNT surface due to weaker PT/CNT interaction as compared to PT/BNNT interaction.

In contrast with observations for BNNTs, no significant color change was evident after addition of the orange-colored rra-P3HT solution to a suspension of hexagonal boron nitride (h-BN) flakes in chloroform (Figure 3a). The absorption spectra of rra-P3HT/h-BN suspensions showed only a small blue shift in comparison to free rra-P3HT (Figure 3b), suggesting a disruption of its  $\pi$ -conjugation by interaction with h-BN, but not the dramatic change observed with BNNTs. These results indicate that h-BN, which is the main impurity in our BNNT samples, does not induce planarization of the rra-P3HT

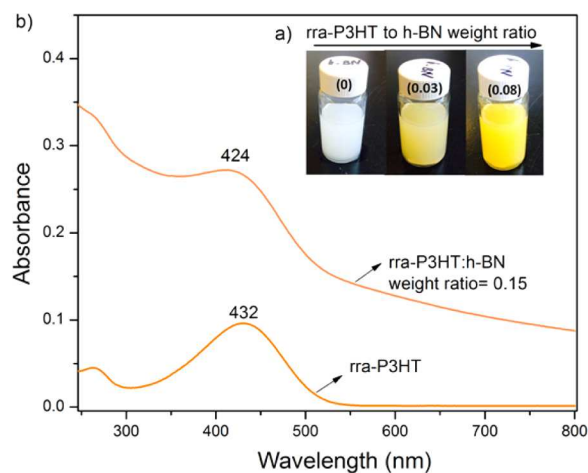


**Figure 3.** (a) Photos of rra-P3HT/h-BN suspensions (0.2 mg/mL) in  $\text{CHCl}_3$  at different rra-P3HT to h-BN weight ratios (indicated by numbers in parentheses) and (b) absorption spectra of rra-P3HT and rra-P3HT/h-BN (0.15 weight ratio) suspensions.

polymer chains at the interface and will not contribute to the intensity of the structured band in the absorption spectra of BNNT samples. Therefore, we conclude that the distinct structured band in the absorption spectra, associated with the planar rra-P3HT, can be used for assessment of the relative purity of BNNT samples.

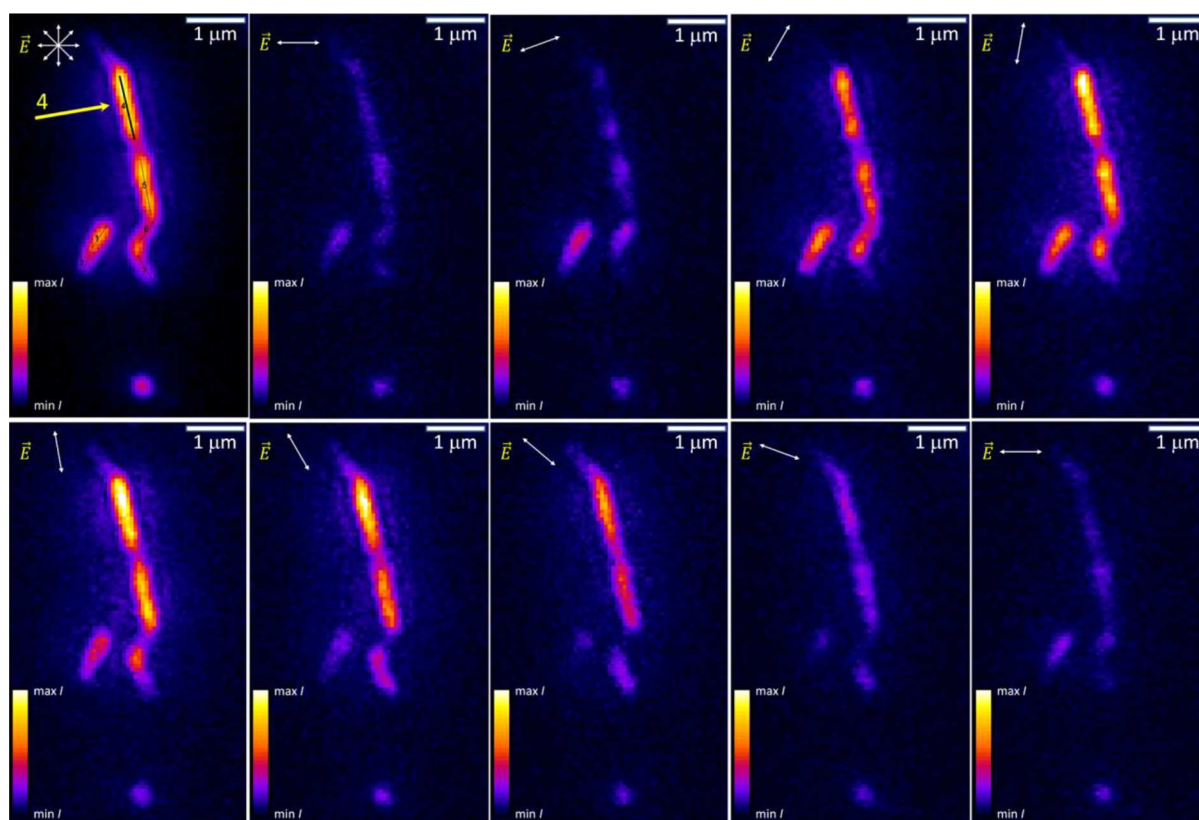
**Polarized Excitation Fluorescence Microscopy.** To elucidate the conformation of the rra-P3HT polymer, highly dilute samples of rra-P3HT/BNNT were imaged by polarized excitation fluorescence microscopy. A similar technique has previously been used to determine single P3HT chain conformation in a PMMA matrix but not in the case of nanotubes.<sup>18</sup> Fluorescence images were recorded as a function of the excitation beam polarization rotated in the 0–180° range in 10 or 20° steps. A similar technique has recently been used in our laboratories to visualize model membrane reorganization and measure order parameters.<sup>19,20</sup>

Figure 4 illustrates the fluorescence intensity variation of rra-P3HT/BNNT fragments with the excitation beam polarization indicated by the  $\vec{E}$  vector. The observation that entire elongated fragments (identified as rra-P3HT-functionalized BNNTs) follow the same intensity variation with excitation polarization indicates a highly anisotropic polymer morphology. The stack of images of varying excitation polarization angle (e.g., Figure 4) was automatically scanned pixel-by-pixel, and the fluorescence intensity as a function of a polarization angle was fitted to eq 1

$$I(x) = I_{\text{bg}} + A \cos^2(x - \alpha) \quad (1)$$

where  $I_{\text{bg}}$  is a local background intensity,  $A$  is the fluorescence intensity modulation amplitude,  $x$  is a laser beam polarization angle, and  $\alpha$  is the excitation dipole moment angle (Figure 5) to obtain the best estimates of the parameters for each pixel.

In addition, a fluorescence intensity modulation depth,  $M = A/I_{\text{avr}}$ , where  $I_{\text{avr}}$  is a background corrected average fluorescence intensity, was calculated. In conjugated polymers like P3HT, the  $M$  value ranges from 1 for chromophores aligned in a stretched chain to 0 for chromophores randomly oriented in a folded chain. Figure 6 shows the intensity variation averaged over the full length of one linear rra-P3HT/BNNT fragment ( $\sim 1 \mu\text{m}$ ) and the best fit to eq 1.



**Figure 4.** Fluorescence intensity variation of rra-P3HT on BNNT as a function of the excitation beam polarization state ( $\vec{E}$  vector in the corner of each image); the top left image corresponds to unpolarized light excitation (the arrow indicates fragment #4).

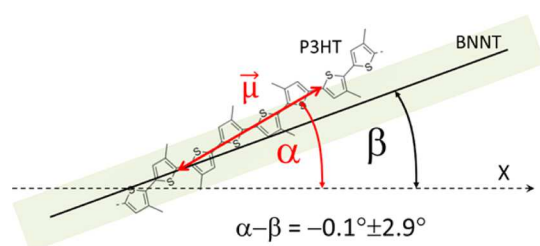


**Figure 5.** Schematic diagram of a P3HT fragment bound to a BNNT ( $\alpha$  and  $\beta$  are the orientation angles of the excitation dipole moment ( $\vec{\mu}$ ) and the BNNT axis, respectively).

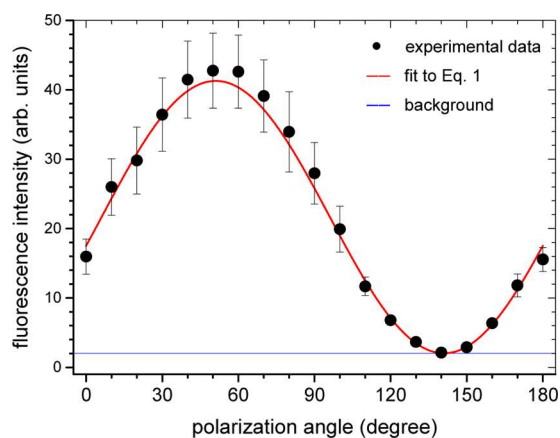


**Figure 6.** Measured fluorescence intensity as a function of polarization angle for a one-pixel-wide line average along fragment #4 in Figure 4.

A set of five new result images was created with pixel values equal to  $I_{\text{avr}}$ , and best estimates of  $A$ ,  $\alpha$ ,  $M$ , and  $r^2$  of the fit ( $A$ ,  $\alpha$ ,  $M$  are shown in Figure 7a, b, and c, respectively). These parameter-mapping images were used together with the polarization resolved image sequences to identify well-separated rra-P3HT/BNNT fragments.

The orientation angles,  $\beta$  (Figure 5), of the linear fragments were measured to determine the BNNT orientation. Systematic measurement of  $\beta$  (Table 1) for both long straight fragments and relatively short ones resulted in the average difference between  $\alpha$  and  $\beta$  angles equal to  $-0.1 \pm 2.9^\circ$ . When only

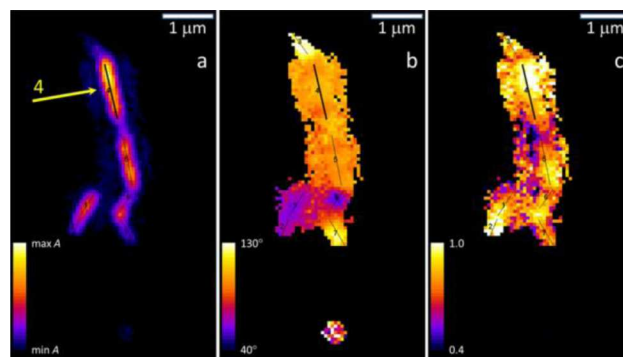


**Figure 7.** Parameter mapping images corresponding to the fluorescence images of rra-P3HT/BNNT (Figure 4). (a–c) Fluorescence intensity amplitude ( $A$ ), excitation dipole moment angle ( $\alpha$ ), and modulation ( $M$ ) obtained from pixel-by-pixel fits to eq 1. BNNT orientation is indicated by the numbered line segments, with an arrow indicating fragment #4.

**Table 1.** rra-P3HT Excitation Dipole Moment and BNNT Orientation Angles  $\alpha$  and  $\beta$  (in degrees) for Three Groups of Linear rra-P3HT/BNNT Fragments along with Their Modulation Depth,  $M$ , and  $r^2$ <sup>a</sup>

	$\alpha$	$\beta$	$M$	$r^2$
1a	112.8 (3.0)	111.5 (1.6)	0.82 (0.02)	0.98 (0.01)
2a	133.4 (0.9)	133.3 (0.6)	0.90 (0.02)	0.96 (0.02)
3a	131.5 (2.7)	130.7 (2.5)	0.84 (0.02)	0.96 (0.01)
1b	60.5 (1.8)	56.6 (2.4)	0.88 (0.05)	0.98 (0.01)
2b	66.7 (1.0)	66.8 (2.4)	1.00 (0.07)	0.96 (0.01)
3b	120.7 (2.9)	126.3 (2.4)	0.91 (0.04)	0.95 (0.03)
4b	103.8 (0.8)	103.9 (2.4)	0.96 (0.01)	0.99 (0.01)
5b	97.2 (2.4)	101.3 (2.4)	0.80 (0.04)	0.98 (0.02)
6b	56.4 (2.2)	54.1 (2.4)	0.82 (0.06)	0.93 (0.03)
7b	120.2 (2.8)	120.1 (2.4)	0.80 (0.04)	0.89 (0.03)
1c	14.0 (0.6)	12.9 (2.4)	0.90 (0.01)	0.98 (0.01)
2c	52.0 (0.5)	50.4 (1.2)	0.96 (0.01)	0.99 (0.01)
3c	44.4 (0.4)	47.2 (2.2)	0.84 (0.01)	0.99 (0.01)

<sup>a</sup>Standard uncertainties are shown in parentheses. Fragments 1b–7b are shown in Figure 7.

relatively long ( $>1-2 \mu\text{m}$ ) and straight fragments were analyzed, the standard uncertainty of the  $\alpha-\beta$  difference could be reduced by a factor of 2 or more. For the linear and isolated BNNT fragments, the intensity modulation depth was generally  $\sim 0.9-1.0$  ( $\sim 90-100\%$  intensity modulation depth; for example, fragment #4 in Figures 4 and 7 and the corresponding graph in Figure 6), which is consistent with the linear rra-P3HT conformation.<sup>18</sup> The effectively  $0^\circ$   $\alpha-\beta$  difference indicates, in turn, that rra-P3HT linearly stretches along BNNTs rather than across. It should be noted that a helical wrapping of BNNTs by the polymer would show qualitatively different intensity variation with two maxima and a reduced modulation depth and thus can be ruled out.

We also observed multiple features with the longest dimension usually below or near the diffraction limit. Some show high modulation depth in the 0.9–1.0 range and are believed to be short rra-P3HT/BNNT fragments, while others exhibit a rather shallow modulation generally less than 0.5, for example, the fragment at the bottom of the images in Figure 4 and the parameter mapping images in Figure 7 (see Figure 8 for intensity variation as a function of the polarization angle). The

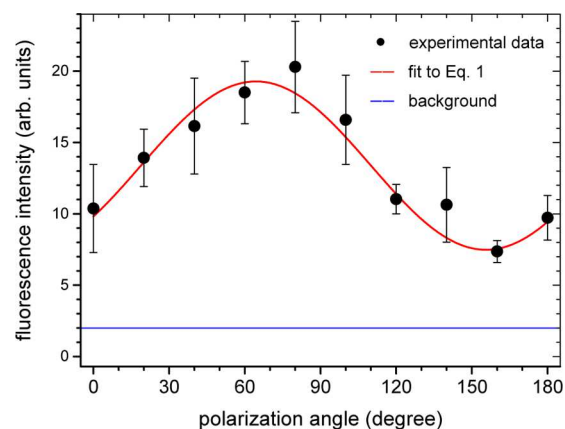


**Figure 8.** Fluorescence intensity variation as a function of polarization angle for the circular feature at the bottom of the images in Figures 4 and 7.

fluorescence features with small modulation depth and ill-defined dipole moment angle are believed to be polymer-covered BN impurities (see Figure 3), which are seen in TEM images (Figure S3).

Several tens of linear fragments, briefly examined but not analyzed in detail for Table 1, all displayed qualitatively equivalent fluorescence dependence on excitation light polarization, leading us to conclude that the rra-P3HT was always planarized and stretched parallel to the long axis of the BNNTs.

## CONCLUSION

We have shown that rra-P3HT is an effective dispersant for BNNTs that self-assembles stretched along the nanotube and improves the solubility of nanotubes in organic solvents. The conformational change generates a distinctive concentration-dependent feature in the absorption spectra of the P3HT/BNNTs hybrid. The rra-P3HT to BNNT weight ratio can be optimized by monitoring absorption signatures for free and bound rra-P3HT, which also establishes a basis for a method for relative assessment of the purity of BNNT samples. We demonstrated polarized excitation fluorescence microscopy to be a powerful tool to elucidate the polymer conformation on nanotubes. Fluorescence imaging allows for visualization of the nanotubes, making it easy to identify their orientation while imaging at optical magnifications. Furthermore, imaging and analysis through a full rotation of the polarization direction provides for an objective assessment of polymer chain morphology on the BNNTs. Although we only directly observe the polymer, evidence from the UV–vis spectra indicated that the majority of the polymers observed were attached to BNNTs. Extensions of this technique are likely to be amenable to studying a variety of nanotube-conjugated polymer interactions and offer obvious advantages in terms of quantitative assessment and representative sampling over more commonly employed imaging techniques.

## ASSOCIATED CONTENT

### Supporting Information

The Supporting Information is available free of charge on the ACS Publications website at DOI: 10.1021/acs.jpcc.5b09049.

Video clip showing variation in fluorescence intensity through a 360 degree rotation of the electric field direction (AVI)

Absorption spectra, TEM, and surface coverage calculations (PDF)

## AUTHOR INFORMATION

### Corresponding Author

\*E-mail: Benoit.Simard@nrc-cnrc.gc.ca. Tel: 613-990-0977.

### Author Contributions

Y.M.R. and Z.J.J. contributed equally to this work. The manuscript was written through contributions of all authors. All authors have given approval to the final version of the manuscript.

### Notes

The authors declare no competing financial interest.

## ACKNOWLEDGMENTS

We thank Dr. Keith Ingold for his helpful comments. This work was supported by the NRC Security Materials Technology Program.

## REFERENCES

- (1) Pal, S.; Vivekchand, S. R. C.; Govindaraj, A.; Rao, C. N. R. Functionalization and Solubilization of BN Nanotubes by Interaction with Lewis Bases. *J. Mater. Chem.* **2007**, *17*, 450–452.
- (2) Wang, W.; Bando, Y.; Zhi, C.; Fu, W.; Wang, E.; Golberg, D. Aqueous Noncovalent Functionalization and Controlled Near-Surface Carbon. *J. Am. Chem. Soc.* **2008**, *130*, 8144–8145.
- (3) Zhi, C.; Bando, Y.; Tang, C.; Xie, R.; Sekiguchi, T.; Golberg, D. Perfectly Dissolved Boron Nitride Nanotubes Due to Polymer Wrapping. *J. Am. Chem. Soc.* **2005**, *127*, 15996–15997.
- (4) Velayudham, S.; Lee, C. H.; Xie, M.; Blair, D.; Bauman, N.; Yap, Y. K.; Green, S. A.; Liu, H. Noncovalent Functionalization of Boron Nitride Nanotubes with Poly(p-phenylene-ethynylene)s and Polythiophene. *ACS Appl. Mater. Interfaces* **2010**, *2*, 104–110.
- (5) Singh, I.; Bhatnagar, P. K.; Mathur, P. C.; Kaur, I.; Bharadwaj, L. M.; Pandey, R. Optical and Electrical Characterization of Conducting Polymer Single Walled Carbon Nanotube Composite Films. *Carbon* **2008**, *46*, 1141–1144.
- (6) Ikeda, A.; Nobusawa, K.; Hamano, T.; Kikuchi, J. Single-Walled Carbon Nanotubes Template the One-Dimensional Ordering of a Polythiophene Derivative. *Org. Lett.* **2006**, *8*, 5489–5492.
- (7) Imin, P.; Cheng, F.; Adronov, A. Supramolecular Complexes of Single Walled Carbon Nanotubes with Conjugated Polymers. *Polym. Chem.* **2011**, *2*, 411–416.
- (8) Bernardi, M.; Giulianini, M.; Grossman, J. C. Self-Assembly and Its Impact on Interfacial Charge Transfer in Carbon Nanotube/P3HT Solar Cells. *ACS Nano* **2010**, *4*, 6599–6606.
- (9) Giulianini, M.; Waclawik, E. R.; Bell, J. M.; De Crescenzi, M.; Castrucci, P.; Scarselli, M.; Diociauti, M.; Casciardi, S.; Motta, N. Evidence of Multiwall Carbon Nanotube Deformation Caused by Poly(3-hexylthiophene) Adhesion. *J. Phys. Chem. C* **2011**, *115*, 6324–6330.
- (10) Liu, J.; Zou, J.; Zhai, L. Bottom-up Assembly of Poly(3-hexylthiophene) on Carbon Nanotubes: 2D Building Blocks for Nanoscale Circuits. *Macromol. Rapid Commun.* **2009**, *30*, 1387–1391.
- (11) Luo, Y.; Santos, F. A.; Wagner, T. W.; Tsoi, E.; Zhang, S. Dynamic Interactions between Poly(3-hexylthiophene) and Single-Walled Carbon Nanotubes in Marginal Solvent. *J. Phys. Chem. B* **2014**, *118*, 6038–6046.
- (12) Liu, J.; Moo-Young, J.; McInnis, M.; Pasquinnelli, M. A.; Zhai, L. Conjugated Polymer Assemblies on Carbon Nanotubes. *Macromolecules* **2014**, *47*, 705–712.
- (13) Kim, K. S.; Kingston, C. T.; Hrdina, A.; Jakubinek, M. B.; Guan, J.; Plunkett, M.; Simard, B. Hydrogen-Catalyzed, Pilot-Scale Production of Small-Diameter Boron Nitride Nanotubes and Their Macroscopic Assemblies. *ACS Nano* **2014**, *8*, 6211–6220.
- (14) Inganas, O.; Salaneck, W. R.; Osterholm, J. E.; Laakso, J. Thermochromic and Solvatochromic Effects in Poly(3-Hexylthiophene). *Synth. Met.* **1988**, *22*, 395–406.
- (15) Heffner, G. W.; Pearson, D. S. Molecular Characterization of Poly(3-hexylthiophene). *Macromolecules* **1991**, *24*, 6295–6299.
- (16) Guo, Y.; Jiang, L.; Ma, X.; Hu, W.; Su, Z. Poly(3-hexylthiophene) Monolayer Nanowhiskers. *Polym. Chem.* **2013**, *4*, 4308–4311.
- (17) Nasrabadi, A. T.; Foroutan, M. Interactions between Polymers and Single-Walled Boron Nitride Nanotubes: A Molecular Dynamics Simulation Approach. *J. Phys. Chem. B* **2010**, *114*, 15429–15436.
- (18) Adachi, T.; Brazard, J.; Ono, R. J.; Hanson, B.; Traub, M. C.; Wu, Z.-Q.; Li, Z.; Bolinger, J. C.; Ganesan, V.; Bielawski, C.; et al. Regioregularity and Single Polythiophene Chain Conformation. *J. Phys. Chem. Lett.* **2011**, *2*, 1400–1404.
- (19) Ngo, A. T.; Jakubek, Z. J.; Lu, Z.; Joós, B.; Morris, C. E.; Johnston, L. J. Membrane Order Parameters for Interdigitated Lipid Bilayers Measured Via Polarized Total-Internal-Reflection Fluorescence Microscopy. *Biochim. Biophys. Acta, Biomembr.* **2014**, *1838*, 2861–2869.
- (20) Carter-Ramirez, D. M.; Jakubek, Z. J.; Lu, Z.; Ogilvie, W. W.; Johnston, L. J. Changes in Order Parameters Associated with Ceramide-Mediated Membrane Reorganization Measured Using pTIRFM. *Langmuir* **2013**, *29*, 15907–15918.